Proceedings Paper:
Pesce, C. orcid.org/0000-0003-0266-0689, Baral, A., Utton, C. et al. (4 more authors) (2023) Effect of synthesis conditions, Zn doping and Al/Fe ratio on calcium [alumino] ferrite structure. In: Thailand Concrete Association, (ed.) Further Reduction of CO2 -Emissions and Circularity in the Cement and Concrete Industry. 16th International Congress on the Chemistry of Cement 2023 (ICCC2023), 18-22 Sep 2023, Bangkok, Thailand. International Congress on the Chemistry of Cement (ICCC) , pp. 94-97.

ICCC 2023 - Guidelines for citation and reuse

Please cite the conference proceedings as following:
Thailand Concrete Association, Ed. *Further Reduction of CO2 -Emissions and Circularity in the Cement and Concrete Industry, 16th International Congress on the Chemistry of Cement 2023 - ICCC2023* (Bangkok 18.-22.09.2023). Bangkok, 2023. Available at: https://www.iccc-online.org/archive/

Please cite individual papers as following:
Author. Title. In: Thailand Concrete Association, Ed. *Further Reduction of CO2 -Emissions and Circularity in the Cement and Concrete Industry, 16th International Congress on the Chemistry of Cement 2023 - ICCC2023* (Bangkok 18.-22.09.2023). Bangkok, 2023. Available at: https://www.iccc-online.org/archive/

The 16th International Congress on the Chemistry of Cement 2023 (ICCC2023)
"Further Reduction of CO_2 -Emissions and Circularity in the Cement and Concrete Industry"
September 18–22, 2023, Bangkok, Thailand

Effect of Synthesis Conditions, Zn Doping and Al/Fe Ratio on Calcium [Alumino] Ferrite Structure

C. Pesce*, A. Baral, C. Utton, H. Kinoshita, N.A. Morley, J. L. Provis, T. Hanein

Department of Materials Science and Engineering, The University of Sheffield, Sheffield, UK
Email: c.pesce@sheffield.ac.uk; a.baral@sheffield.ac.uk; c.utton@sheffield.ac.uk; h.kinoshita@sheffield.ac.uk; n.a.morley@sheffield.ac.uk; j.provis@sheffield.ac.uk; t.hanein@sheffield.ac.uk

ABSTRACT
The use of steel waste for clinker production is a promising solution to reduce the environmental impact of Portland cement. While it is known that clinker produced from steel slag shows some advantageous properties e.g., lower burning temperature and reduced use of limestone, it is necessary to understand the formation and stability of iron-rich clinkers doped with the minor elements commonly found in steel wastes. In this study, pure ferrite phases were synthesized with varying Al/Fe ratios, burning temperature, cooling regimes, and in the presence of Zn as a minor element at various dosages. The phase assemblage and microstructure of the obtained ferrites were characterised by XRD/Rietveld and BSE-SEM/EDX. The results show that Zn is partially incorporated into the ferrite structure and partially replaces Al to form a Ca-Al-Zn phase. The Zn-incorporated ferrite leads to increased lattice parameter due to the bigger ionic radius of the dopant with respect to the substituted ions, and to increased crystallinity due to the increased ion mobility brought by ZnO which acts like a flux.

KEYWORDS: *Ferrite, Clinker, Zinc, Cooling rate, Firing temperature*

1. Introduction

Cement production is the major contributor to CO_2 emissions in the construction industry and accounts for 8% of total CO_2 emissions. Peys et al (2022) have recently proposed that the use of Fe-rich materials for cement production can be advantageous due to their ability to lower the clinkering temperature and to their cementitious properties, so far essentially unexplored, whilst upcycling largely available Fe-rich industrial by-products and residues, such as steel slags and bauxite residues. Fe in clinkers is usually found in the calcium [alumino] ferrite (or ferrite) phase, a solid solution with formula $Ca_2Fe_{2-x}Al_xO_5$ with $x \leq 1.4$. Only a few studies have been carried out on the synthesis of pure ferrite phases. In a ternary system CaO-Al_2O_3-Fe_2O_3, the final phase assemblage of ferrites is influenced by the Al/Fe ratio, burning temperatures, cooling rates, and the presence of minor elements in the raw materials. Ferrite accommodates substitution by different elements, including Zn, Mg, and Ti (Peys et al 2022; Murat and Sorrentino 1996; Chabayashi et al 2012). Zn is found in many of the major Fe-rich side streams potentially beneficial to use for clinker production (Peys et al 2022). In clinkers, Zn is known to be mainly incorporated in the aluminate and ferrite phases forming substitutional solid solutions. There is contradictory information regarding the solubility limit of Zn in clinkers, reported at 0.5-1 wt% (Barbarulo, Sorrentino, and Sing 2007), 2 mol% in C_4AF and 5 mol% in C_2F (Shevchenko and Jak 2019) and 0.7 wt% (Gineys et al 2011). Formation of C–Z–A phases has been reported in ferrites at Zn dosage ≥1.0 wt% (Bolio-Arceo and Glasser 1998; Barbarulo, Sorrentino, and Sing 2007; García-Díaz et al 2008) and >0.7 wt%. Understanding ferrite behaviour under different sintering conditions is key for the design of clinkers produced from Fe-rich resources and there is a clear need to gain insights on the effects of Zn as a minor element in clinkers. In this study, ferrites are synthesised at high temperatures varying Zn dosage, Al/Fe ratio, burning temperature, and cooling method, and characterised by powder X-ray diffraction (XRD)/Rietveld and scanning electron microscope/energy-dispersive X-ray spectroscopy (SEM/EDS) to obtain information on the phase assemblage, microstructure, and Zn distribution.

2. Materials and methods

Commercial reagents were used for the synthesis of ferrites: Al_2O_3 ≥99.7% (Thermo Scientific Chemicals), $Fe^{3+}{}_2O_3$ ≥96% (Sigma-Aldrich), $CaCO_3$ ACS reagent grade (Sigma-Aldrich), and ZnO 99.9% (Sigma-Aldrich). Mixtures were prepared at different A/F ratios within the $Ca_2(Fe_{2-x}Al_x)O_5$ solid solution at x=0, 0.33, 1, 1.67. For Zn-doped samples, the same mixtures were used and ZnO was added to the mixtures at 0.5 wt%, 1.0 wt%, and 2.0 wt%. The mixtures (~80g each batch) were prepared by weighing the reagents in the selected proportions and dry-mixing using a Retsch PM 100 ball mill. The mixtures were placed in a ZrO_2 80 mL jar with ZrO_2 ø 5 mm balls, and milled for 10 min at 200 rpm. The ground mixtures were then pressed into ø 16 mm pellets using a manual pellet press. The high-temperature synthesis was carried out in an electric muffle furnace at different firing temperatures (T_f): 1250°C, 1300°C and 1350°C. For all syntheses, the sample pellets were placed in a Pt crucible and put in the furnace at 900°C, then ramped up to the selected T_f at a heating rate of 5°C/min and dwelt at the selected T_f for 1 hour. Two cooling methods were studied: i) fan-assisted air quenching (AQ); ii) water quenching (WQ), carried out by taking the Pt crucibles containing the samples out of the furnace and placing them in a shallow stainless steel tray filled with water, so that only the crucible comes in contact with water but not the sample. The synthesised products were stored in a desiccator filled with silica gel until analysis. Table 1 shows the list of ferrites targetted. Hereinafter, samples are denominated after the target phase, ZnO wt%, firing temperature, and cooling method. For example, a mixture of C_4AF target doped with 1.0 wt% ZnO, fired at 1350°C and air quenched will be called C_4AF-1-1350-AQ.

The synthesis products were characterised by XRD. The instrument was a Panalytical X'Pert^3 Powder equipped with an Empyrean Cu tube (λ=1.54187 Å) used under the following operating conditions: 45 kV tube voltage, 40 mA tube current, 0.016726°2θ/s scan speed, 0.0131303°2θ step size, and 10-70°2θ scan range. The samples were manually ground with an agate pestle and mortar until all material could pass a 63 µm sieve. The powders were back-loaded to the sample holder, which was set to rotate at 15 rpm during the analysis. The phase analysis was carried out with the ICDD PDF4+/Sieve+ software. The Rietveld method interfaced with Diffrac.Topas 6 was used to perform Quantitative Phase Analysis (QPA) and to refine space group, crystallite size and strain, and lattice parameters. Analysis by SEM/EDS was performed on a polished cross-section of sample C_4AF-0.5-1350-AQ. To produce the polished surface, a broken fracture of the pellet was placed on a fitted plastic mould with the cross section facing the bottom. The mould was filled with a 3:1 v/v mixture of epoxy resin and hardener (Buehler EpoThin 2 resin and hardener) and cured at ambient conditions overnight. The mounted sample was ground and polished with a Buehler Automet 250 automatic grinder-polisher. Grinding steps were performed on SiC discs with increasing grit sizes of 220, 320, 400, and 600 and ethanol was used as lubricant. Polishing steps were performed on Buehler polishing cloths using diamond suspensions with sizes 15, 6, 3, 1, and 0.25 µm (MetPrep) and oil-based diamond lubricant (MetPrep). The polished section was carbon coated (10 nm) and stored in a desiccator until analysis. SEM/EDS analysis was performed on an FEI Inspect F50 equipped with an Oxford Instruments EDS detector. Images were taken in secondary electron/back-scattered electron modes at a voltage of 15.0 kV.

Table 1. List of synthesised ferrites. T_f=firing temperature; AQ=air quenched; WQ=water quenched.

A/F ratio $Ca_2Fe_{2-x}Al_xO_5$	Target phase	T_f (°C)	ZnO wt%	Cooling method
x=0	C_2F	1350	0.0/2.0	AQ
x=0.33	C_6AF_2	1350	0.0/2.0	AQ
x=1	C_4AF	1250	0.0/2.0	AQ
		1300	0.0/2.0	AQ
		1350	0.0/2.0	AQ/WQ
			0.5/1.0	AQ
x=1.67	C_6A_2F	1350	0.0/2.0	AQ

3. Results and discussion

Figure 1 shows the XRD diffractograms of ferrite samples. The highest intensity peaks of the (141) reflections of brownmillerite and the (100) of srebrodolskite were selected to evaluate shifts. In Figure 1a, the (141) peaks of brownmillerite show a slight shift towards wider d-spacing with increasing %wt Zn. This is likely due to the bigger ionic radius of Zn^{2+} (0.6-0.9 Å) with respect to Fe^{3+} (0.49-0.78 Å) (Shannon 1976). The Rietveld refinement of lattice parameters shows a monotonic increase in lattice parameter along the b axis. In Figure 1b, the (141) reflections of brownmillerite and the (100) of srebrodolskite show a

pronounced shift towards narrower d-spacing with increasing A/F ratio, both for undoped and Zn-doped ferrites. This is consistent with a Fe^{3+} substitution by the smaller Al^{3+} (ionic radius 0.39-0.535 Å) (Shannon 1976). Interestingly, all C-A-F phases show a slight shift towards wider d-spacing when doped with Zn however, the C_2F phase shows a slight shift towards smaller d-spacing when doped with Zn. This trend change is likely related to the space group change occurring at x~0.2-0.4 from *Pnma* (srebrodolskite) to *Ibm*2 (brownmillerite) and to the higher number of VI-coordinated Fe^{3+} ions (0.55-0.645 Å ionic radius) present in the srebrodolskite structure. Substitution with IV-coordinated Zn^{2+} (0.60 Å) would explain the observed reduction in the lattice parameter in Zn-doped C_2F. In Figure 1c, the effect of varying firing temperatures is shown. The position of the (141) reflection of brownmillerite does not show any significant trend with increasing firing temperatures, while the crystallinity increases with the firing temperature, and increases pronouncedly in the Zn-doped ferrites. The Rietveld crystallite size shows an increase from ~20 nm in the undoped ferrite fired at 1250°C to ~70 nm in the undoped ferrite fired at 1350°C. The increase in crystallite size in the Zn-doped ferrites is less pronounced. The results suggest that the presence of Zn is the major contributor with respect to firing temperatures in increasing the crystallinity. This is likely because ZnO acts as a flux, increasing the melt content (García-Díaz et al 2008; Andrade, Maringolo, and Kihara 2003) and therefore the kinetics of nucleation and growth of high-temperature phase crystals is increased with respect to a solid state reaction. In Figure 1d, the (141) reflections of brownmillerite in air-quenched and water-quenched ferrites are compared. It is confirmed that the presence of Zn is accompanied by a pronounced increase in crystallinity however, no clear effect of the cooling method on the brownmillerite structure could be observed.

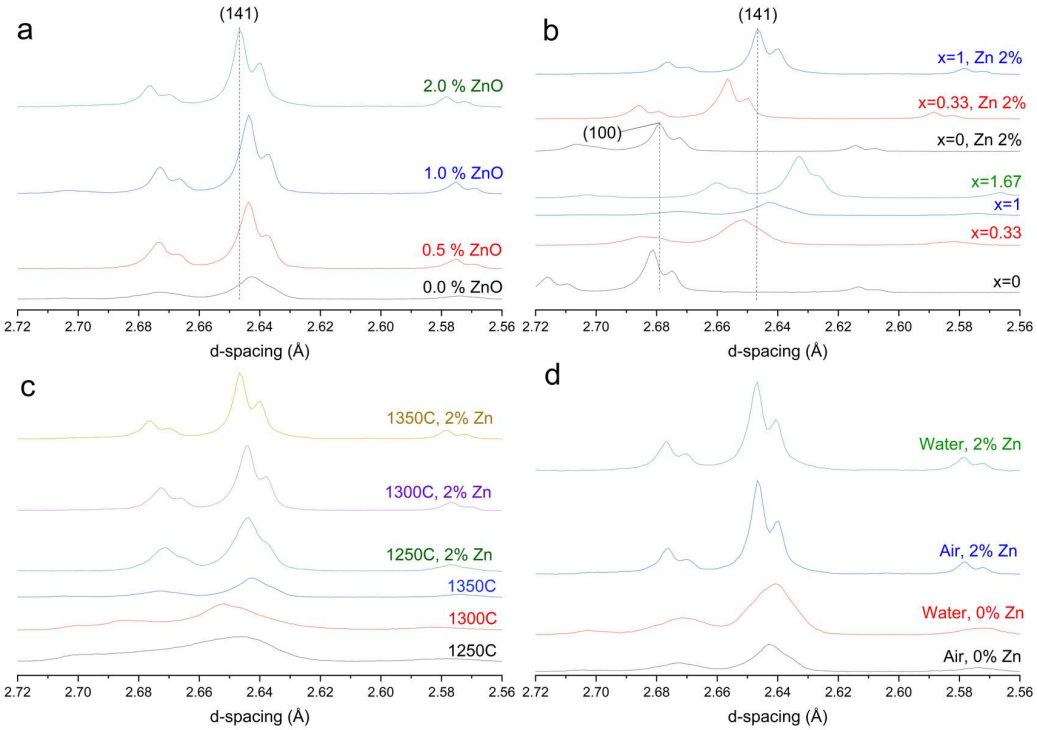

Figure 1. XRD scans showing the (141) reflections of brownmillerite (for C-A-F samples) and (100) reflection of srebrodolskite (for C_2F samples) in various conditions: a) increase in lattice parameter with increasing ZnO% of C_4AF-1350-AQ; b) decrease in lattice parameter with increasing A/F ratio of ferrites fired at 1350°C and air quenched; c) increase in crystallinity with increasing firing temperature and presence of Zn in C_4AF-AQ samples; d) no clear effect of cooling method (air quenched/water quenched) in C_4AF-1350.

The EDS mapping of a 30×26 µm area on the polished surface of sample C_4AF-0.5-1350-AQ is shown in Figure 2, displaying the mapping of elements Ca, Al, Fe, and Zn, along with the corresponding back-scattered electrons (BSE) image. The elements distribution does not appear homogeneous and there are areas where there is a higher concentration of Ca and Fe and other areas rich in Al and Zn. Two phases can be distinguished from the analysis: a major phase that is Ca-rich and has similar amounts of Fe and Al with traces of Zn, and a secondary phase Al-rich and with minor amounts of Ca and Zn. The major phase is consistent with a C_4AF phase doped with Zn, as expected by the stoichiometry of raw materials used and

confirmed by the brownmillerite pattern shown by XRD, with a slight shift towards wider d-spacing caused by the bigger ionic radius of Zn^{2+} replacing Al or Fe (Figure 1a). The secondary phase shows an average atomic composition determined by EDS similar to krotite ($CaAl_2O_4$) partially substituted by Fe ~2% and Zn ~1%. The secondary phase might also be part of the solid solution $Ca_{12}Al_{9-y}Zn_{5+x}O_{32\pm\delta}$, x = 5–5.76 and y = 8.1–8.73 (Kahlenberg and Krüger 2022). However, neither the main peak for krotite nor the main peak of $Ca_6Zn_3Al_8O_{15}$, which is the (044) reflection at 2.6350 Å (Bolio-Arceo and Glasser 1998), were detected in our XRD measurements. Furthermore, the formation of C-Z-A phases has been reported to start at higher Zn dosages, such as 1% (Bolio-Arceo and Glasser 1998; Barbarulo, Sorrentino, and Sing 2007; García-Díaz et al 2008) and 0.7% (Gineys et al 2011).

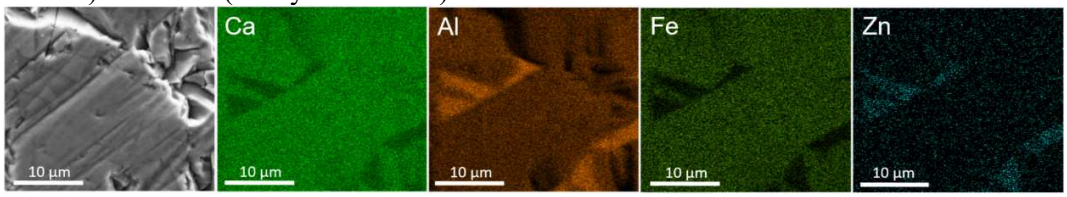

Figure 2. Back-scattered micrograph (left) and EDS mapping of elements Ca, Al, Fe, and Zn on the polished section of C_4AF-0.5-1350-AQ.

4. Conclusions

The effects of Zn on ferrite reported in the literature are often contradictory. In this study, Zn-doped ferrites were synthesised at varying conditions of A/F ratio, burning temperature, Zn dosage, and cooling method. The main findings are that i) Zn is incorporated in ferrites and its presence leads to an increase in lattice parameter due to the larger ionic radius of Zn^{2+} with respect to Al^{3+}, which on the contrary causes a decrease in lattice parameter with increasing A/F ratio. Higher firing temperatures and Zn dosages result in an increase in crystallinity, likely due to the higher melt content which aids crystallisation. No clear effects were observed in relation to the cooling method. Zn preferentially replaces Al in a Ca-Zn-Al phase.

Acknowledgements

This work was supported by the Engineering and Physical Sciences Research Council [grant number EP/W018810/1].

5. References

Andrade, F.R.D., V. Maringolo, and Y. Kihara. 2003. "Incorporation of V, Zn and Pb into the crystalline phases of Portland clinker", *Cement and Concrete Research*, 33: 63-71.

Barbarulo, R., F. Sorrentino, and C. Sing. 2007. "Impact of ZnO on clinker composition and reactivity-Coupling with MgO." *12th International Congress on the Chemistry of Cement*. Montreal, Canada.

Bolio-Arceo, H, and F.P. Glasser. 1998. "Zinc oxide in cement clinkering: part 1. Systems CaO-ZnO-Al_2O_3 and CaO-ZnO-Fe_2O_3", *Advances in Cement Research*, 10(1): 25-32.

Chabayashi, T., A. Nakamura, H. Kato, and K. Sada. 2012. "Influence of titanium oxide and magnesium oxide on the mineral composition and the properties of cement", *Cement Science and Concrete Technology*, 66(1): 211-16.

García-Díaz, I., F. Puertas, M. F. Gazulla, M. P. Gómez, and M. Palacios. 2008. "Effect of ZnO, ZrO_2 and B_2O_3 on clinkerization process. Part I. Clinkerization reactions and clinker composition", *Materiales de Construcción*, 58(292): 81-99.

Gineys, N., G. Aouad, F. Sorrentino, and D. Damidot. 2011. "Incorporation of trace elements in Portland cement clinker: Thresholds limits for Cu, Ni, Sn or Zn", *Cement and Concrete Research*, 41: 1177-84.

Kahlenberg, V., and H. Krüger. 2022. "High-temperature behavior and structural studies on $Ca_{14}Al_{10}Zn_6O_{35}$", *Zeitschrift für Kristallographie*, 237(6-7): 219-32.

Murat, M., and F. Sorrentino. 1996. "Effect of large additions of Cd, Pb, Cr, Zn, to cement raw meal on the composition and the properties of the clinker and the cement", *Cement and Concrete Research*, 26(3): 377-85.

Peys, A., V. Isteri, J. Yliniemi, A. S. Yorkshire, P. N. Lemougna, C. Utton, J. L. Provis, R. Snellings, and T. Hanein. 2022. "Sustainable iron-rich cements: Raw material sources and binder types", *Cement and Concrete Research*, 157: 106834.

Shannon, R. D. 1976. "Revised effective ionic radii and systematic studies of interatomic distances in halides and chalcogenides", *Acta Crystallographica*, A32: 751-67.

Shevchenko, M., and E. Jak. 2019. "Experimental Liquidus Studies of the CaO-ZnO-Fe_2O_3 System in Air", *Journal of Phase Equilibria and Diffusion*, 40: 779-86.